Spectral variation of the volume scattering function measured over the full range of scattering angles in a coastal environment

Malik Chami, Eugeny B. Shybanov, Gueorgui A. Khomenko, Michael E.-G. Lee, Oleg V. Martynov, and Gennady K. Korotaev

The spectral volume scattering function (VSF) was measured in a coastal environment from 0.6° to 177.3° by use of a recently developed device. The spectral variations of the particulate VSF and phase function (i.e., ratio of the VSF to the scattering coefficient) were examined as a function of the scattering angle. The angular dependency of both VSF and phase-function spectra was highly sensitive to the absorption and to the size distribution of the particles. As a result, the use of spectrally neutral phase functions in radiative-transfer modeling is questioned. © 2006 Optical Society of America

OCIS codes: 010.4450, 290.5850, 290.1350.

1. Introduction

The volume scattering function [VSF, hereafter denoted $\beta(\theta)$, where θ is the scattering angle] describes the angular distribution of the light scattering that results from an incident beam interacting with an infinitesimally small volume of water. It is a fundamental inherent optical property for understanding marine optics. For example, with regard to satellite remote-sensing applications, knowledge of the VSF together with the absorption coefficient and the surface boundary conditions (wind, state of the sea) allows a prediction of the water-leaving radiance to be made, which is of primary importance for deriving biogeochemical parameters such as chlorophyll concentration. One can also use the VSF measurements to obtain information about the nature of the particulate matter in the oceans, such as the refractive index and the size distribution of particles. Several models that rely on scattering properties were developed to estimate the bulk refractive index of particles.[1–10] For most of these models, the particulate backscattering ratio (i.e., the ratio of the particulate backscattering coefficient to the particulate scattering coefficient) is the key parameter. This is so because this ratio is highly sensitive to both the composition of the particles and their size. For example, minerals, bubbles,[11,12] and submicrometric[13] particles typically induce high values of the backscattering ratio, whereas phytoplankton and large cells exhibit low values of this ratio.

Despite its fundamental nature, the range of variability of the VSF in the ocean remains largely unknown, mainly because of practical difficulties in achieving direct VSF measurements. Most of the available measurements were carried out decades ago.[14–17] Owing to the lack of VSF data, a typical approach to radiative-transfer modeling has consisted of using an averaged particulate phase function derived from Petzold's data[15] to predict the water-leaving signal. The decision to use an average phase function was also made to facilitate numerical intercomparisons among radiative transfer models.[18] Nevertheless, such an approach is questionable because phytoplankton, detritus, bubbles, and resuspended sediment, which all have different optical properties, contribute to the VSF of the particles. Another way to overcome the lack of VSF measurements consists of using models, such as Mie theory, to compute the particles' VSFs. This way of computation, however, requires knowledge of the bulk refractive index and the size distribution

M. Chami (chami@obs-vlfr.fr) is with the Laboratoire Océanographie de Villefranche, Unité Mixte de Recherche Associée au Centre National de la Recherche Scientifique 7093, Villefranche sur Mer, France. E. B. Shybanov, M. E.-G. Lee, O. V. Martynov, and K. Korotaev are with the Marine Hydrophysical Institute, National Academy of Sciences, Ukraine. G. A. Khomenko is with the Laboratoire d'Océanographie Côtière du Littoral, Ecosystèmes Littoraux et Côtiers, Université du Littoral Côte d'Opale, France.

Received 22 April 2005; revised 22 October 2005; accepted 24 October 2005.

0003-6935/06/153605-15$15.00/0

of the particles. The bulk refractive index (relative to the refractive index of seawater) usually used for phytoplankton and minerals ranges from 1.02 to 1.07 (Refs. 19–21) and from 1.14 to 1.26,[22,23] respectively, whereas the relative refractive index of bubbles is 0.75. A power law (Junge distribution) is often used to approximate the particle size distribution.[11,24–26] Other models based on bimodal size distribution have also been developed[27–29] to separate the contribution of the small, supposedly mineral, particles from the large biogenic particles.

To overcome the lack of data, several instruments to measure $\beta(\theta)$ *in situ* were recently designed. The Hydroscat-6 (HOBILabs) instrument[30] provides $\beta(\theta)$ at a single scattering angle, namely, 140°, at six wavelengths. The ECO-VSF (WETLabs) instrument measures $\beta(\theta)$ at three scattering angles (100°, 125°, and 150°) at a single wavelength. The volume scattering meter[31] (VSM) is a novel instrument that measures the VSF in the ocean over nearly the complete angular range of the scattering angles, thus allowing measurements of the phase functions of the particles to be made. In spite of their large differences in design and calibration, the three instruments mentioned above showed agreement within 10% during an intercomparison exercise.[10]

Despite the fact that VSF measurements are now possible with this new generation of devices, results related to the variability of the VSF in the open ocean and coastal waters remain scarce. The VSM instrument was recently used in a multispectral mode in a coastal environment, namely, the Crimea Peninsula in the Black Sea.[32] For the first time, the volume scattering function was measured at various wavelengths (i.e., 443, 490, and 555 nm) in a range of scattering angles of 0.6°–177.3°. In the present paper we focus on the angular dependency of the spectral variation of the VSF and the phase function of particles; the latter currently remains limited to relatively few determinations. The paper is organized as follows: First, the protocols used for the absorption and scattering measurements are described. Then the spectral variations of the VSF and the phase function are presented and discussed. The influence of the absorption and the size distribution of particles on the spectral shapes of the VSF is examined.

2. Material and Methods

The data analyzed in this study were collected from an oceanographic platform located 600 m offshore the southern coast of the Crimea Peninsula in the Black Sea. Seawater samples (132 in total) were collected from 27 July to 15 August 2002 at depths of 0, 4, 8, 12, 16, and 20 m at 11 h local time. The notation and abbreviations used to describe this study in the balance of this paper are listed in Appendix A.

A. Chlorophyll and Absorption Measurements

The chlorophyll a concentrations (hereafter referred to as Chl a) and the particulate absorption measurements were carried out following the ocean optics protocols recommended for the satellite ocean color sensor validation.[33] Chl a was determined by use of the standard fluorometric method.[34]

The absorption coefficients of the particles were measured based on the methods described by Yentsch[35] and by Mitchell and Kiefer.[36] The separation of the particulate absorption into phytoplankton and other components is based on the methanol extraction method.[37] The measurement made before the extraction with methanol provides the total particulate absorption coefficient a_p, while the depigmented particle absorption coefficient a_{NAP} is obtained after extraction. The parameter a_{NAP} is consistent with absorption by the detrital particulate matter and is thus referred to as the nonalgal particle absorption coefficient. Phytoplankton absorption coefficient a_{ph}, which represents absorption by living particles, is obtained as the difference between a_p and a_{NAP}. Details of the protocols used for the Chl a and absorption measurements are provided by Chami *et al.*[32]

B. Scattering Measurements

1. Volume Scattering Meter

The measurements of the VSF were carried out with the VSM instrument, which was developed at the Marine Hydrophysical Institute (Ukraine) in cooperation with Satlantic, Inc. (Canada).[31] The VSM has already been described by Lee and Lewis.[31] The main features of the instrument are summarized in this section. The VSM provides measurements of the VSF with an angular resolution of 0.3° (from 0.6° to 177.3°). The concept of the instrument differs from traditional approaches inasmuch as the positions of the light source and the photodetector are fixed. The measurement angle is modified by rotation of a special periscope prism with three reflecting facets. The shape of the prism, together with precise design geometry, allows the scattered radiance to be detected practically over the full angular range. The beam divergence is 0.1°, and the receiver acceptance angle is 0.2°. When the measurement angle is equal to zero, the instrument permits the measurement of beam-attenuation coefficient c. The VSF is extrapolated in the near-forward direction to 0° through a power-law dependency.[38] The integration of $\beta(\theta)$ provides scattering coefficient b [Eq. (1)] and backscattering coefficient b_b [Eq. (2)]:

$$b = 2\pi \int_0^{\pi} \beta(\theta)\sin\theta \mathrm{d}\theta \left[\mathrm{m}^{-1}\right], \tag{1}$$

$$b_b = 2\pi \int_{\pi/2}^{\pi} \beta(\theta)\sin\theta \mathrm{d}\theta \left[\mathrm{m}^{-1}\right]. \tag{2}$$

The normalization of $\beta(\theta)$ by the scattering coefficient yields phase function $\tilde{\beta}$:

$$\tilde{\beta}(\theta) = \frac{\beta(\theta)}{b} \quad \left[\mathrm{sr}^{-1}\right]. \tag{3}$$

To obtain the VSF of the particles, $\beta_p(\theta)$, we subtracted the contribution of pure seawater to VSF from the measurements by applying the coefficients provided by Morel.[39] The correction for salinity was carried out according to the method of Boss and Pegau.[40]

For the first time to our knowledge, the VSM instrument was used in a multispectral mode. This was possible because the design of the VSM allows a filter wheel to be added in front of the receiver. Three spectral filters, centered at 443, 490, and 555 nm with a bandpass of 20 nm at full width at half-maximum, were employed. The VSM was operated in benchtop mode on the discrete samples on the platform. The subsamples from the same Niskin bottle used for the Chl *a* and absorption measurements were introduced into the chamber of the VSM for analysis, providing us with concurrent measurements of VSF, Chl *a*, and particulate absorption.

2. Calibration of the Volume Scattering Meter

Because the VSM is still a new instrument that has not been extensively used in field experiments, its calibration is worth describing in detail.

Signal $S(\lambda, \theta)$ recorded in relative units by a computer can be expressed as

$$S(\lambda, \theta) = P(\lambda, \theta)B_s(\lambda, \theta) \quad [\text{counts}], \tag{4}$$

where λ is the wavelength, θ is the scattering angle, $B_s(\lambda, \theta)$ [W nm^{-1} sr^{-1}] is the radiance of scattered light incident onto the photodetector, and $P(\lambda, \theta)$ [counts (W nm^{-1} sr^{-1})$^{-1}$] is a coefficient that describes the conversion of light energy into counts.

Scattered light $B_s(\lambda, \theta)$ [W nm^{-1} sr^{-1}] is proportional to incident flux $\phi(\lambda)$ [W nm^{-1}]:

$$B_s(\lambda, \theta) = G(\lambda, \theta)\phi(\lambda) \quad [\text{W nm}^{-1}\,\text{sr}^{-1}]. \tag{5}$$

Function $G(\lambda, \theta)$ [sr^{-1}] depends on the geometry of the sampling chamber and on the beam-attenuation coefficient. Combining Eqs. (4) and (5), we can write

$$S(\lambda, \theta) = G(\lambda, \theta)\phi(\lambda)P(\lambda, \theta) = G(\lambda, \theta)K(\lambda, \theta). \tag{6}$$

In Eq. (6), $G(\lambda, \theta)$ does not depend on the incident flux. $K(\lambda, \theta)$ [counts sr] is the calibration coefficient. The calibration procedure consists in determining coefficient $K(\lambda, \theta)$.

Function $G(\lambda, \theta)$ is written as

$$G(\lambda, \theta) = 4\pi\beta(\lambda, \theta)V(\theta)\exp[-cL(\theta)] \quad [\text{sr}^{-1}], \tag{7}$$

where $V(\theta)$ [m] is the average path length within the scattering volume. The scattering volume is the intersection between the viewing cone of the detector and the light beam. $V(\theta)$ is calculated as the ratio of the scattering volume [m^3] to the cross section of the light beam [m^2]. In Eq. (7), $L(\theta)$ [m] is the path length of the photon from the illuminator to the detector, c [m^{-1}] is the beam-attenuation coefficient, and $\beta(\lambda, \theta)$ is the VSF [m^{-1} sr^{-1}].

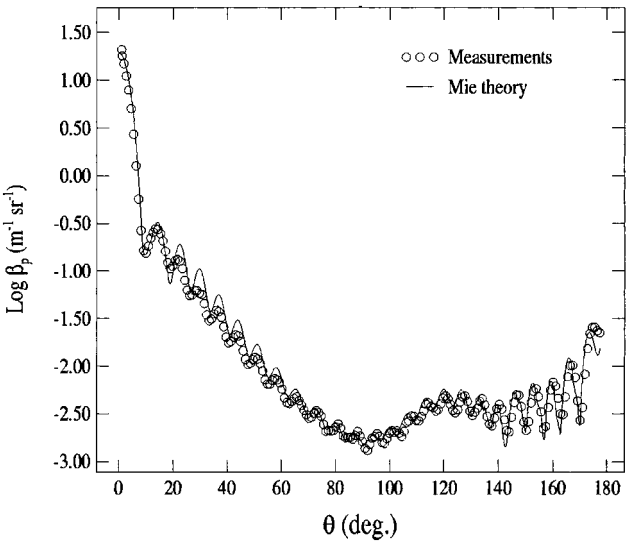

Fig. 1. Comparison of measurements of the VSF with Mie theory: example for monodispersed spheres of size 3 μm at 490 nm.

Scattering volume $V(\theta)$ and photon path length $L(\theta)$ are computed theoretically from the geometrical parameters of the device, including the position of the prism. The theoretical calculations provide values of $V(\theta)$ in the full range of scattering angles (i.e., from 0° to 180°), allowing the VSF to be processed in the near-forward and near-backward directions. Attenuation coefficient c is derived from the measurement of the intensity[31] of the light at 0°. Therefore, given wavelength λ and scattering angle θ, calibration coefficient $K(\lambda, \theta)$ can be derived from Eqs. (6) and (7) if the values of $\beta(\lambda, \theta)$ are known at any angles. Using the subscript cal to refer to a calibration experiment, we express $K(\lambda, \theta)$ as

$$K(\lambda, \theta) = \frac{S_{\text{cal}}(\lambda, \theta)}{4\pi\beta_{\text{cal}}(\lambda, \theta)V(\theta)\exp[-c_{\text{cal}}L(\theta)]} \quad [\text{counts sr}]. \tag{8}$$

Practically, the calibration was carried out as follows: The chamber of the VSM instrument that contains the sample was filled with a suspension of artificial particles that consisted of latex polystyrene microspheres of precisely known size and refractive index ($n_1 = 1.59$). A set of beads size ranging from 0.6 to 160 μm was used. Because the particles are nearly perfectly spherical, their VSF can be predicted with high accuracy from Mie theory. Therefore the beads provide a means to calibrate the instrument. Calibration coefficient $K(\lambda, \theta)$ was estimated by the least-squares method based on minimization of the difference between the logarithms of the measured and the simulated signals. The observations of the VSF of beads compared well with theoretical Mie calculations (Fig. 1). The uncertainty in $\beta(\theta)$ based on the calibration experiment was less than 10% for

each wavelength: The relative error was 5.7 at 443 nm, 4.8% at 490 nm, and 5.2 at 555 nm. A post-deployment calibration, which was carried out just after the field campaign, revealed that the instrument did not drift.

When the calibration is made and coefficient $K(\lambda, \theta)$ is known, the spectral volume scattering function of the samples is derived from Eqs. (6) and (7):

$$\beta(\lambda, \theta) = \frac{S(\lambda, \theta)}{4\pi K(\lambda, \theta) V(\theta) \exp[-cL(\theta)]} \quad [\mathrm{m}^{-1}\,\mathrm{sr}^{-1}]. \tag{9}$$

3. Results and Discussion

The variability in the Chl *a* concentration and in the optical properties of the particles (i.e., absorption, scattering, and backscattering coefficients) observed during the field experiment was discussed by Chami *et al.*[32] Briefly, Chl *a* varied from 0.45 to 2.1 mg m^{-3}, as was typical of summer conditions. The nonalgal particles' absorption contributed 40% to as much as 88% at 443 nm to the total particulate absorption. The values of the backscattering ratio of the particles, $\tilde{b}_{bp}$ (i.e., defined as the ratio of the backscattering coefficient to the scattering coefficient), varied in the range 1.2%–3.2%. The spectral shapes of scattering coefficient b_p, backscattering coefficient b_{bp}, and backscattering ratio $\tilde{b}_{bp}$ of particles often showed a significant depression (~20%) in the blue relative to the green. In what follows, we discuss the spectral variation of the VSF and the phase function of particles.

A. Spectral Variation of the Particulate Volume Scattering Function at 140°

Previous studies[30,32,40,41] showed that $\beta_p(140°)$ could be used to derive the backscattering coefficient b_{bp}. Therefore the analysis of $\beta_p(140°)$ is of particular interest, for example, in remote-sensing studies. So far, the lack of knowledge regarding the spectral behavior of $\beta_p(140°)$ is still important. Figure 2 shows examples of the spectral variation of $\beta_p(140°)$ measured on different days and at several depths during the experiment. To highlight the varying spectral shape of $\beta_p(140°)$, we normalized the values to the value at 555 nm. The dependency of $\beta_p(140°)$ on wavelength showed variable shapes. The examples plotted in Fig. 2 were selected because they are representative of various optical conditions: a weak concentration of chlorophyll *a* (on 29 July at 0 m; Chl $a = 0.6$ mg m^{-3}, a minimum of a_{NAP} [on Aug 1 at 20 m, $a_{\mathrm{NAP}}(443\ \mathrm{nm}) = 0.03\ \mathrm{m}^{-1}$], a maximum of a_{NAP} [on 8 August at 0 m, $a_{\mathrm{NAP}}(443\ \mathrm{nm}) = 0.09\ \mathrm{m}^{-1}$] and a high concentration of chlorophyll *a* (on Aug 11 at 4 m, Chl $a = 1.9$ mg m^{-3}). The spectral ratio $\beta_p(140°, 443\ \mathrm{nm})/\beta_p(140°, 555\ \mathrm{nm})$ varied from 0.7 to 1.20, thus highlighting the difficulty of establishing a general law for the spectral variation of $\beta_p(140°)$. As shown in Fig. 2, the values at 443 nm were generally lower than those at 490 nm, leading to a convex shape of the spectra. The analysis

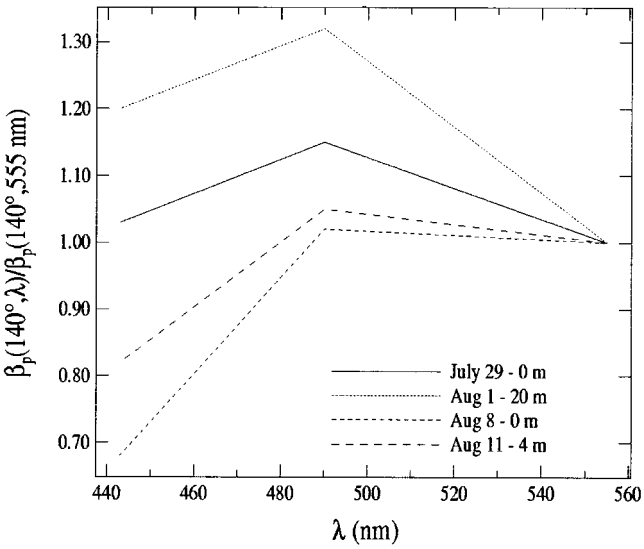

Fig. 2. Spectral variation of the VSF at 140° normalized to 555 nm for several samples.

of the data revealed that the decrease of $\beta_p(140°)$ at 443 nm tended to be more pronounced after 6 August.

These results are not unexpected from both theory and previous measurements.[42–44] The spectral variations of the scattering properties of the particles are sensitive to the absorption effects,[42–44] especially in the vicinity of the absorption bands where the real part of refractive index n_p exhibits weak variations owing to anomalous dispersion.[42,45] More specifically, with increasing wavelength λ, n_p exhibits a dip and then an increase as it passes throughout the absorption band. Such a dip induces a decrease of the scattering coefficient. As a result, high absorption leads to lower scattering. In this study, the mean single scattering albedo of the particles, ω_p, which is defined as the ratio of scattering coefficient b_p to attenuation coefficient c_p, was 0.77 ± 0.07, 0.84 ± 0.04, and 0.92 ± 0.03 at 443, 490, and 555 nm, respectively. The low ω_p values in the blue part of the spectrum underline the strong influence of the absorption on the scattering process, which is consistent with a decrease of $\beta_p(140°)$ in the blue domain, in agreement with the theory of anomalous dispersion. In particular, the observation that $\beta_p(140°, 443\ \mathrm{nm})/\beta_p(140°, 555\ \mathrm{nm})$ was minimum on 1 August at 20 m and maximum on 8 August at 0 m (Fig. 2) is consistent with the magnitude of the measured particulate absorption coefficient. Furthermore, Bricaud and Morel[42] and Ahn *et al.*[43] showed, based on measurements of algae cultures that backscattering efficiency factor Q_{bb} of several species increases with wavelength in the range 400–500 nm. Backscattering efficiency factor Q_{bb} is defined as the ratio of the radiative energy backscattered by the particle to the energy impinging on the geometrical cross section of the same particle. The decrease of Q_{bb} in the blue was ascribed to variations of the absorption properties. As $\beta_p(140°)$ is highly correlated to b_{bp},[30,35] and thus to Q_{bb}, the sensitivity of the measured $\beta_p(140°)$ spectra

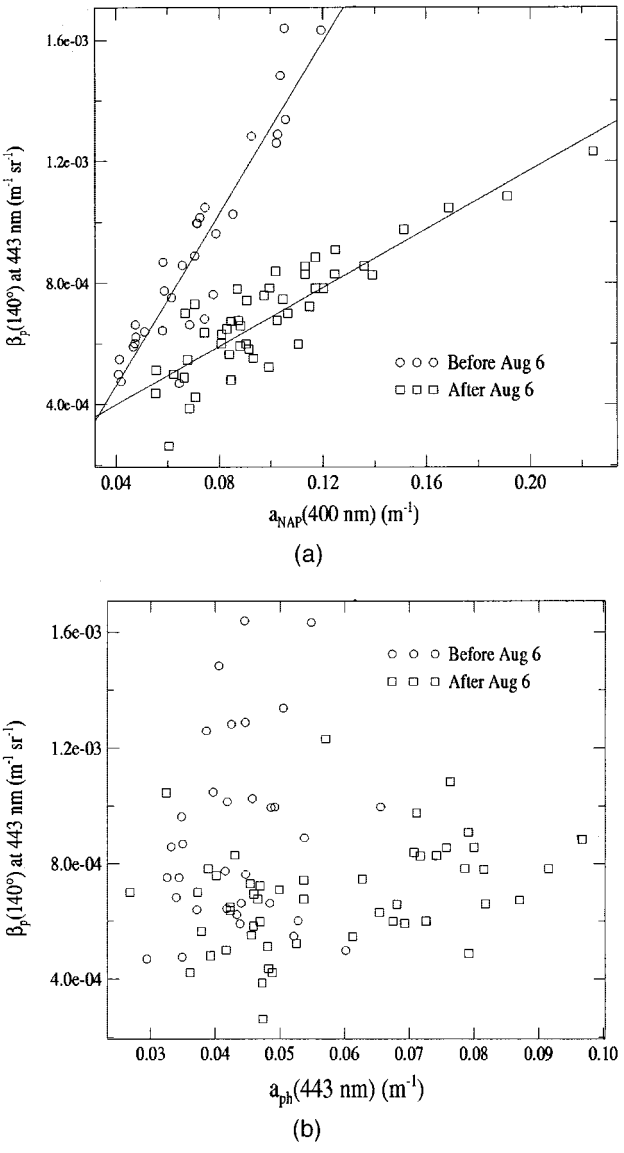

Fig. 3. (a) Relationship between $\beta_p(140°)$ at 443 nm and the absorption coefficient of nonalgal particles a_{NAP} at 400 nm. Equations for the linear fit: before 6 August, $\beta_p(140°, 443\ nm) = 0.0140\ a_{NAP}(400\ nm) - 0.0001$; $r^2 = 0.86$. After 6 August, $\beta_p(140°, 443\ nm) = 0.0048\ a_{NAP}(400\ nm) + 0.0002$; $r^2 = 0.76$. (b) Relationship between $\beta_p(140°)$ at 443 nm and absorption coefficient of phytoplankton a_{ph} at 443 nm.

to the absorption effects is consistent with these experimental observations.

The significant drop of ω_p at 443 nm suggests the presence of colored particles (i.e., more absorbing in the blue domain) in the study area with significant effect on total scattering. The relationship between $\beta_p(140°, 443\ nm)$ and the particulate absorption coefficients was studied. $\beta_p(140°, 443\ nm)$ was found to be significantly correlated with the absorption coefficient of the nonalgal particles, a_{NAP} at 400 nm [Fig. 3(a)], while no significant correlation with the absorption coefficient of phytoplankton a_{ph} at 443 nm was found [Fig. 3(b)]. Therefore the same particles contributing to a_{NAP} were the major contributors to $\beta_p(140°, 443\ nm)$. Because these particles were highly absorbing in the blue (because a_{NAP} increases exponentially with decreasing λ), they were probably responsible for the decline of $\beta_p(140°, 443\ nm)$. Actually, either of two relationships was observed, depending on whether the measurements were collected before 6 August (slope, $0.014\ sr^{-1}$; $r^2 = 0.86$) or after 6 August (slope, $0.0048\ sr^{-1}$; $r^2 = 0.76$). This means that the absorbing particles contributing to $\beta_p(140°, 443\ nm)$ changed during the experiment. After 6 August, the magnitude of $\beta_p(140°, 443\ nm)$ decreased (Fig. 3), meaning that the contributors to the backscattering signal showed a higher ratio of absorption to scattering. The increased absorption efficiency of the particles is corroborated by the significant decrease of $\omega_p(443\ nm)$ after 6 August, with mean values of $\omega_p(443\ nm)$ that varied from 0.82 ± 0.04 before 6 August to 0.73 ± 0.04 after 6 August. Based on the analysis of backscattering ratio $\tilde{b}_{bp}$, Chami *et al.*[32] showed that highly refractive particles, such as minerals, were the primary components that influenced the backscattering coefficient in the study area. Therefore mineral particles manifested high variability in their absorption properties during the experiment. This is not surprising because previous studies[23,46–49] showed that the specific absorption by minerals can vary by more than 1 order of magnitude in natural waters.

The significant variability observed in the absorption properties of the particles during the field campaign was accompanied by an important variability of the angular shape of the VSF as well. At 443 nm, the angular ratio $\beta_p(140°)/\beta_p(90°)$, which is a measure of the asymmetry of the VSF, varied from 0.80 ± 0.07 before 6 August to 0.63 ± 0.05 after 6 August, which means a steepening of the VSF in the backward direction in the second half of the experiment. Additionally, based on the measurements of the phytoplankton's specific absorption coefficient (which is defined as the ratio of phytoplankton absorption to Chl *a*), Chami *et al.*[32] showed that the community structure of phytoplankton also changed after 6 August with the presence of larger cells or cells acclimated to lower light. Therefore both the VSF and the absorption measurements support the idea that the water body changed during the experiment. This change in the water mass was closely related to atmospheric conditions. A low-pressure system passed over the Crimea Peninsula on 6–7 August, producing important changes in the weather leading to an increase of the wind speed to $12\ m\ s^{-1}$. The gusting wind modified the direction of the coastal currents, which was measured with an acoustic Doppler current profiler instrument.[32] The eastern transport of the seawater along the coast observed before 6 August was replaced by a western transport. The advection of a new water mass in the study area probably explains the observed variations in the optical properties of the particles. Based on (i) the geography of the study area, (ii) the direction of the currents after 6 August, and (iii) the fact that optical properties of

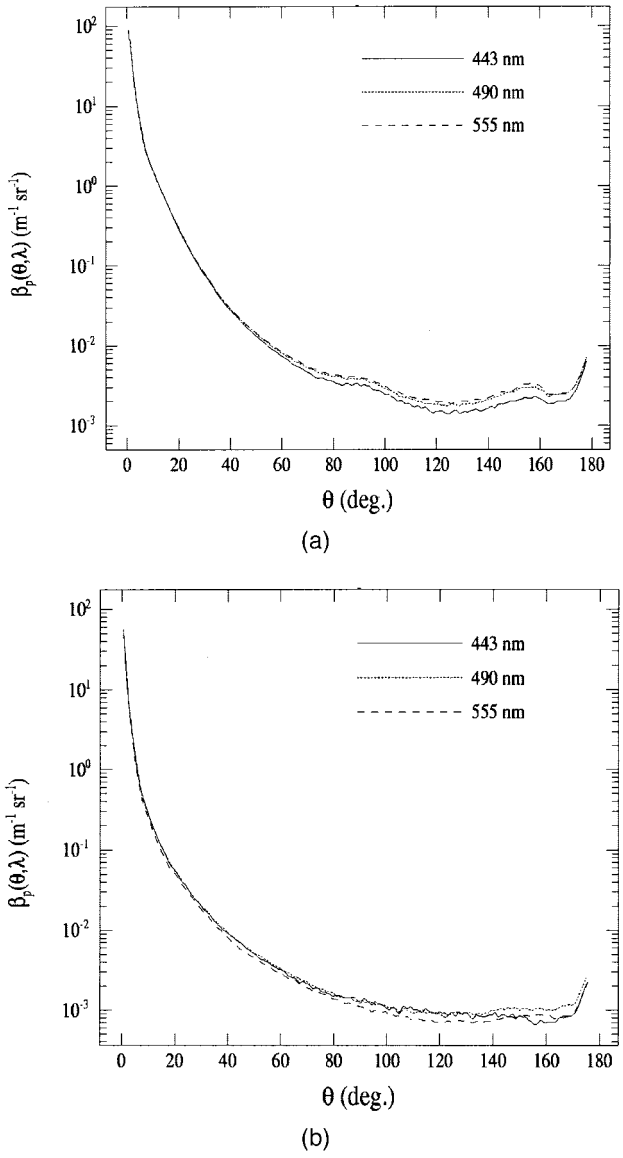

Fig. 4. Examples of spectral variation of the VSF (a) on 30 July at 0 m and (b) on 1 August at 16 m.

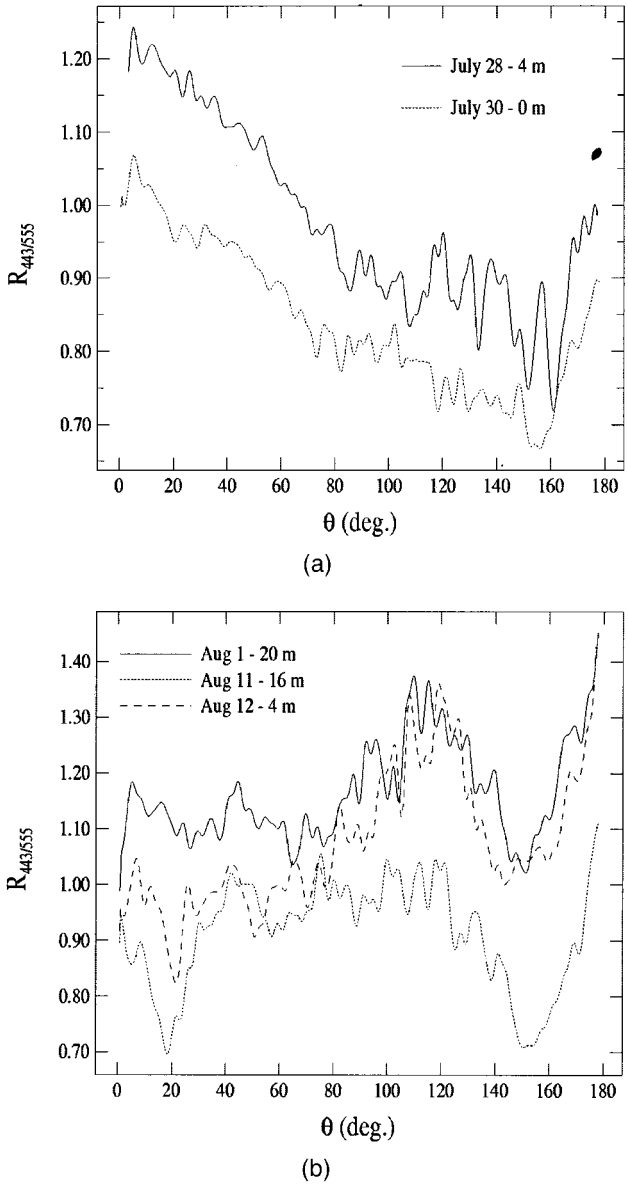

Fig. 5. Dependence of $R_{443/555}$, the spectral ratio of VSF from 443 to 555 nm, on scattering angle as measured on (a) 28 July at 4 m, 30 July at 0 m and (b) 1 August at 20 m, 11 August at 16 m, and 12 August at 4 m.

the particles are typical of the types of coastal waters, we believe that the water body came from the productive Azov Sea.

B. Spectral Variation of the Particulate VSF as a Function of the Scattering Angle

The originality of this study lies in our ability to investigate the spectral variation of the VSF with respect to the scattering angle for the first time based on modern instrumentation. A significant variability of the spectral shape of the VSF was observed during the experiment (Fig. 4), especially in the backward hemisphere. The VSF at 443 nm was widely different from the VSFs at 490 and 555 nm, which were often nearly similar. For example, the VSF was lower in the blue relative to the green from 60° to 177° on 30 July at 0 m [Fig. 4(a)], whereas the opposite behavior of the VSF was observed on 1 August at 16 m, at least up to 150° [Fig. 4(b)]. On the basis of the results obtained for the $\beta_p(140°)$ spectra, the spectral ratio $\beta_p(\theta, 443\ \text{nm})/\beta_p(\theta, 555\ \text{nm})$ [hereafter referred to as $R_{443/555}(\theta)$] is a relevant parameter with which to study the wavelength dependency of the VSF measured at all angles. The measurements showed that $R_{443/555}$ is highly dependent on the scattering angle. In spite of the great variability observed during the experiment, three general shapes of the angular variation of $R_{443/555}$ prevailed (Fig. 5). One shape was characterized by a nearly regular decrease of $R_{443/555}(\theta)$ with increasing θ, as observed on 28 July at 4 m and on 30 July at 0 m [Fig. 5(a)]. The two other shapes showed more-intricate spectral changes. The first exhibited a maximum near 120°, for example on

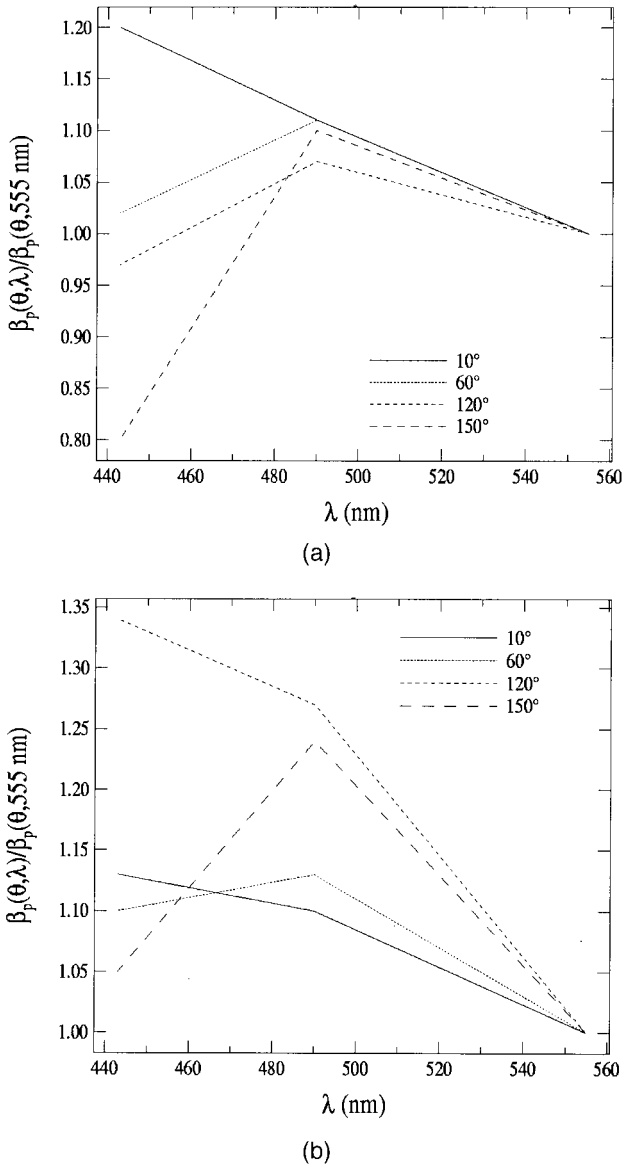

Fig. 6. Spectral variation of β_p normalized to 555 nm measured at four scattering angles, namely, 10°, 60°, 120°, and 150°, on (a) 28 July at 4 m and (b) 1 August at 20 m.

1 August at 20 m and on 12 August at 4 m, while the other shape showed pronounced minima near 20° and 160°, for example on 11 August at 16 m [Fig. 5(b)]. To illustrate better the complex variations of $R_{443/555}(\theta)$, we plotted the β_p spectra for several scattering angles, namely, 10°, 60°, 120°, and 150°, on 28 July at 4 m [Fig. 6(a)] and on 1 August at 20 m [Fig. 6(b)]. On 28 July the β_p spectra showed an increasing reduction in $\beta_p(443\ nm)$ with θ. On 1 August, $\beta_p(\theta)$ was variable and did not show consistent changes with θ.

Because the spectral behavior of $\beta_p(140°)$ was shown to be strongly influenced by the absorption properties of the particles, we investigated whether the angular variations observed in $R_{443/555}(\theta)$ can also be sensitive to the effects of the particulate absorption. Therefore, angular ratio $R_{443/555}(120°)/R_{443/555}(140°)$, which provides information about the magnitude of the decrease of $R_{443/555}$ with θ in the backward direction, was related to parameter a_p/c_p at 443 nm. Because the optical properties of the particles were variable at the surface during the experiment,[32] we first focused on the relationship in the 0–4 m layer. A significant positive correlation was found ($r^2 = 0.76$): $R_{443/555}(120°)/R_{443/555}(140°)$ increases by nearly 30% with increasing a_p/c_p (Fig. 7). Therefore the increased contribution of the particulate absorption to the attenuation coefficient leads to a steeper slope of $R_{443/555}$ with θ. As an example, the highest values of the angular ratio were observed when the data were collected after 6 August, where $a_p/c_p(443\ nm) > 0.2$ [i.e., $\omega_p(443\ nm) < 0.8$]. However, it should be stressed that no correlation was found between $R_{443/555}(120°)/R_{443/555}(140°)$ and $a_p/c_p(443\ nm)$ for the whole data set, thus suggesting that absorption by the particles might not be the only factor influencing the angular shape of $R_{443/555}(\theta)$.

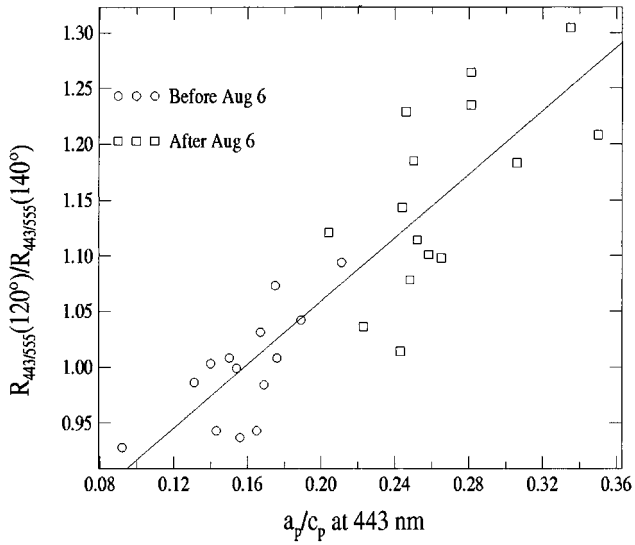

Fig. 7. Relationship between angular ratio $R_{443/555}(120°)/R_{443/555}(140°)$ and parameter a_p/c_p at 443 nm from 0 to 4 m. Linear fit, $R_{443/555}(120°)/R_{443/555}(140°) = 1.42\ a_p/c_p(443\ nm) + 0.77$; $r^2 = 0.76$.

To verify that angular dependency of the spectral ratio could be reproduced from theory, we compared the experimental results with Mie theory. When dealing with *in situ* measurements, one can justify the use of Mie theory because a randomly oriented population of irregularly shaped particles can be well approximated by an equivalent size distribution of spherical particles. We carried out computations for a realistic range of relative refractive-index and particle-size distributions. The real part of relative refractive index n_p varied from 1.02 to 1.20 in steps of 0.01, and the imaginary part, n_p', varied from 0 to 0.01 in steps of 0.0005. We also tested the refractive index of 0.75 to examine the possible influence of bubbles. A Junge hyperbolic size distribution, which often is used for natural waters,[24,40,50,51] was applied as the particle-size distribution. The Junge exponent ξ of the distribution varied from 3.1 to 5.0 in steps of

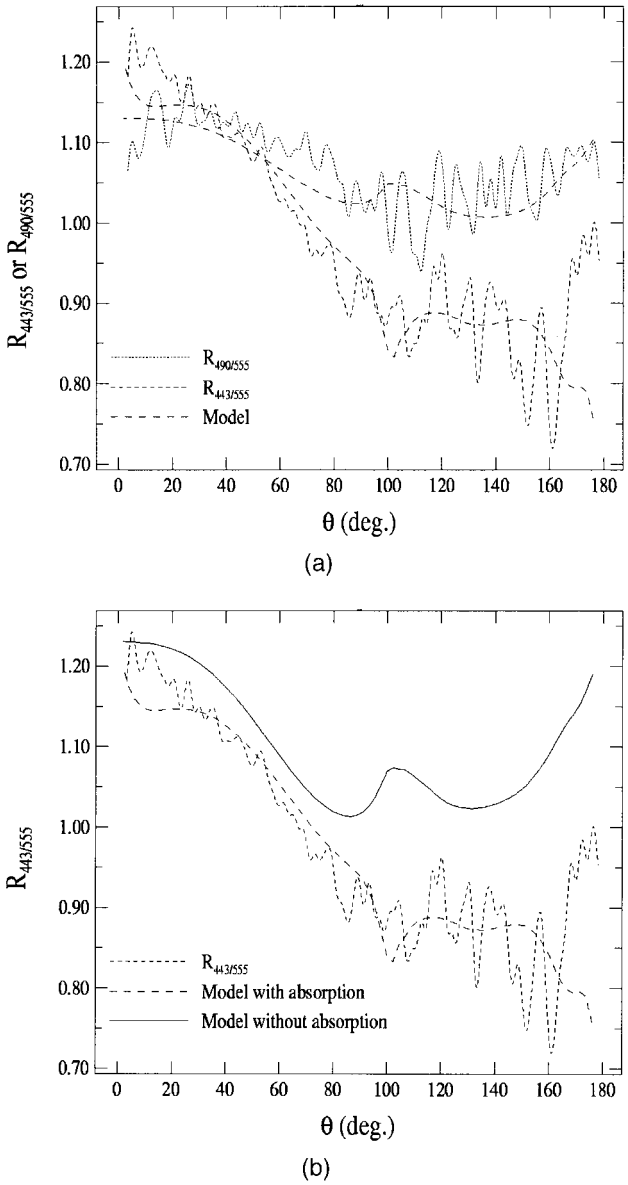

Fig. 8. (a) Retrieval of spectral ratios $R_{443/555}$ and $R_{490/555}$ with Mie theory on 28 July at 4 m. The size distribution of the particles followed a Junge power law. Refractive index of the particles: $n_p = 1.14$; $n_p' = 0.002$ at 443 nm; $n_p' = 0$ at 490 nm. Junge exponent, $\xi = 3.9$. (b) Retrieval of $R_{443/555}$ by use of absorbing and nonabsorbing particles (i.e., $n_p' = 0$).

0.1 in the simulations, and the minimum and maximum radii of the distribution were 0.1 and 40 μm, respectively. The accuracy of the retrieval of the measurements of $R_{443/555}(\theta)$ and $R_{490/555}(\theta)$ [note that $R_{490/555}(\theta)$ is the spectral ratio of β_p from 490 to 555 nm] was estimated from the relative root-mean-square error (RMS), which is defined as

$$\mathrm{RMS} = \left\{\frac{1}{N}\sum_{i=1}^{N}\left[\frac{R_{\lambda/555}(\theta_i)_{\mathrm{estimated}} - R_{\lambda/555}(\theta_i)_{\mathrm{measured}}}{R_{\lambda/555}(\theta_i)_{\mathrm{measured}}}\right]^2\right\}^{1/2}, \quad (10)$$

Table 1. Accuracy of Retrieval of Spectral Ratios $R_{443/555}$ and $R_{490/555}$ with Mie Theory for Representative Measurements of the Data Set Expressed in Terms of Relative RMS (%)

	Date (Depth [m])			
Spectral Ratio	28 July (4)	1 August (20)	11 August (16)	12 August (4)
$R_{443/555}$	5.7	7.0	9.1	6.9
$R_{490/555}$	4.3	8.7	7.6	7.9

where $R_{\lambda/555}(\theta)$ is the parameter being investigated, λ is either 443 or 490, and N is the number of scattering angles. Because our goal was to examine whether the three prevailing spectral shapes of variations in $R_{443/555}$ with θ (as shown in Fig. 5) could be explained by theory, we focused on the retrieval of representative measurements such as those collected on 28 July at 4 m, on 1 August at 20 m, on 11 August at 16 m, and on 12 August at 4 m.

On 28 July, we obtained the best agreement between measurements and computations when the real and imaginary parts of the refractive index were $n_p = 1.14$, $n_p' = 0.002$ at 443 nm and $n_p' = 0$ at 490 nm; and the Junge exponent ξ was 3.9 [Fig. 8(a)]. The RMS of $R_{443/555}(\theta)$ was 5.7% and of $R_{490/555}(\theta)$ was 4.3% (Table 1). Despite the fact that the values of the inputs of Mie computations could not be rigorously validated, it is worth noting that the value of n_p is consistent with the refractive index estimated from backscattering ratio $\tilde{b}_{bp}$ (Ref. 32) by use of the model of Twardowski *et al.*, which was also 1.14. Similarly, a complex refractive index, and thus absorption, was introduced at 443 nm for correctly retrieving the data. We also tested the case of nonabsorbing particles at 443 nm [i.e., $n_p' = 0$; Fig. 8(b)] to quantify the influence of the absorption. The mismatch between the computations and the measurements was significant (RMS, 13.3%). The greatest discrepancies were observed in the backward direction where the calculations of β_p for nonabsorbing particles showed a fairly neutral spectral variation with θ. The influence of absorption on the scattering process was expected to be less in the forward direction because scattering in the forward peak is sensitive more to the size of particles throughout the diffraction phenomena and to a lesser extent to the refractive index of particles. Introduction of absorption allows us to explain the observed decrease of $R_{443/555}$ with θ. Therefore the strong sensitivity of the β_p spectra with the scattering angle to the absorption effects, as observed in the surface layer (Fig. 7), is supported by theory.

We also tried to match the measured angular variation of $R_{443/555}$ with theory for the other prevailing spectral shapes (i.e., those of 1, 11, and 12 August). Despite the introduction of complex refractive indices, the Junge size distribution did not allow us to retrieve the intricate features observed in $R_{443/555}(\theta)$, such as the maximum near 120° or the minima near 20° and 160°. As we previously inferred by the lack

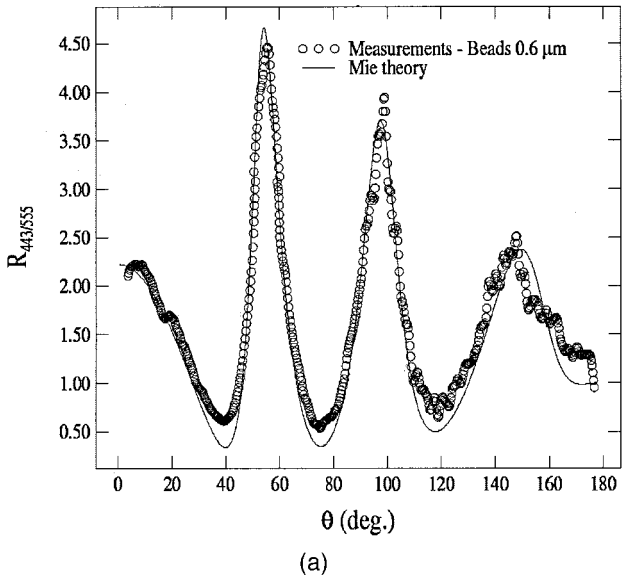

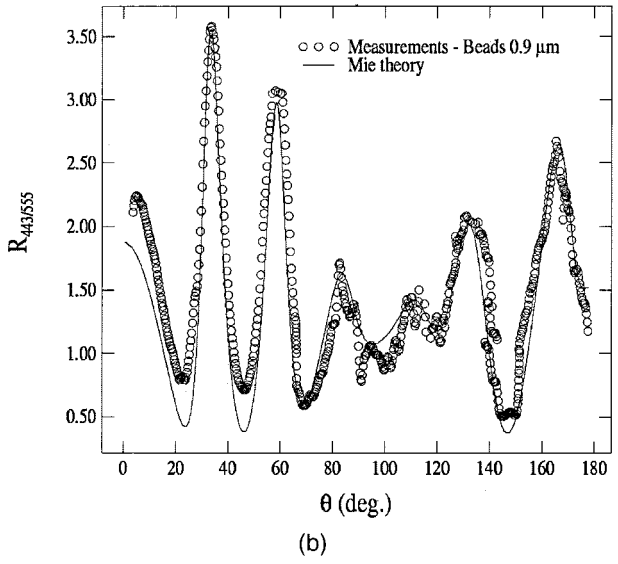

Fig. 9. Angular distribution of spectral ratio $R_{443/555}$ observed during the calibration experiment for beads sizes (a) 0.6 and (b) 0.9 μm. Results from Mie theory are also shown.

of correlation between angular ratio $R_{443/555}(120°)/R_{443/555}(140°)$ and $a_p/c_p(443\ \text{nm})$ with regard to the whole data set, the angular variation of the β_p spectra does not seem to be exclusively sensitive to the absorption effects. The size distribution of the particles might also be a source of variability in the angular distribution of $R_{443/555}$. To examine the influence of the size distribution, we studied the data obtained with monodispersed beads during the calibration experiment. The calibration measurements are helpful for two reasons: The size distribution follows a lognormal function and thus differs from the Junge power law, and the imaginary part of the refractive index of the beads is known to be small and thus the calibration data are not altered by the effects of absorption. Examples of variations in $R_{443/555}(\theta)$ measured for two bead sizes,

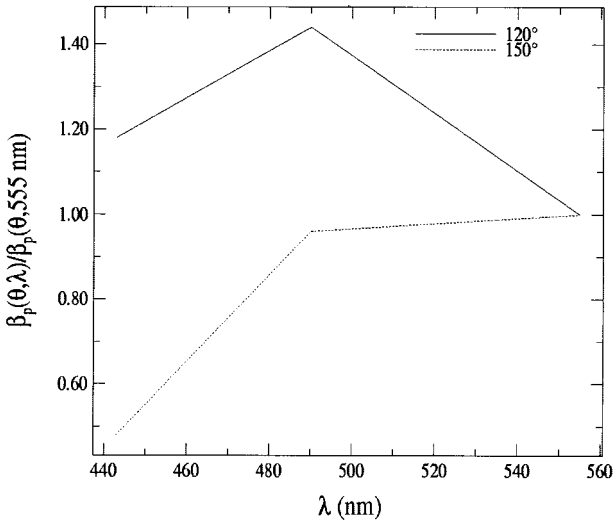

Fig. 10. Example of β_p spectra normalized to 555 nm at 120° and 150° when the bead size is 0.9 μm.

namely, 0.6 and 0.9 μm, are plotted in Fig. 9. In both cases, $R_{443/555}(\theta)$ showed strong features, with successions of maxima and minima, which were well reproduced by Mie theory. Oscillations in $R_{443/555}(\theta)$ value mean that the β_p spectra could vary sharply within a small range of scattering angles. As an example, β_p shows a greater spectral slope from 443 to 555 nm at 150° than at 120° when the bead size is 0.9 μm (Fig. 10).

Therefore the calibration data suggest that the maxima and minima observed in the measurements of $R_{443/555}(\theta)$ on 1, 11, and 12 August could possibly be retrieved by use of Mie theory, provided that a modal distribution of the particles is introduced into the computations. Practically, because a single monodispersed mode of particles is not realistic in natural waters, the size distribution of the particles was described as the sum of a Junge law and a lognormal function. The lognormal size distribution typically characterizes the presence of monodispersed particles, whereas the Junge law is representative of a continuous background of particles. It should be highlighted that such a model of size distribution was previously shown to be relevant for the Baltic Sea.[52] The presence of monodispersed particles could also be relevant near the platform because the structure of the water column is continuously changed at such a near-coastal site, even during calm conditions, by a complex system of currents, narrow jets, etc. We adjusted the parameters of the lognormal distribution (real and imaginary parts of refractive indices m_p and m_p', mean radius r_{mean}, and standard deviation σ) to retrieve the measurements. Note that a complex refractive index was used in the modal distribution to account for the absorption properties of the monodispersed particles.

On 11 August at 16 m, the best agreement between theory and measurements (Fig. 11) was obtained for the following parameter values: The refractive indices of the particles distributed according to the Junge

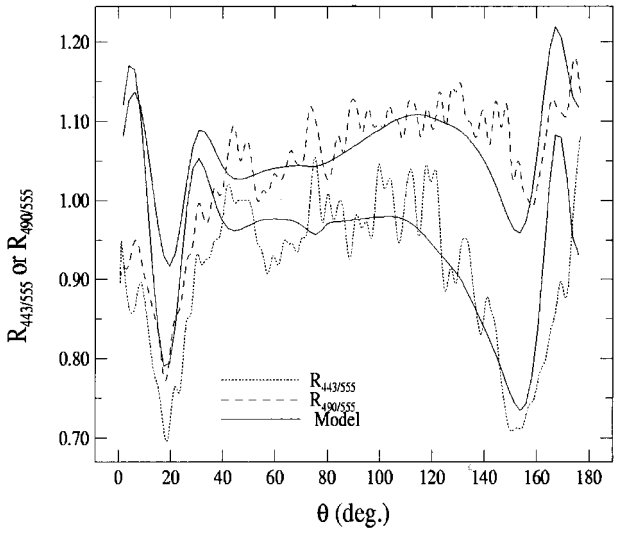

Fig. 11. Retrieval of spectral ratios $R_{443/555}$ and $R_{490/555}$ with Mie theory on 11 August at 16 m. The size distribution was modeled as the sum of a Junge power law and a lognormal function. Refractive indices corresponding to particles distributed according to the Junge law, $n_p = 1.07$ and $n_p' = 0.0002$; the Junge exponent, ξ, 3.2; refractive indices of particles lognormally distributed, $m_p = 1.17$ and $m_p' = 0.007$ at 443 nm and $m_p' = 0.0005$ at 490 nm; mean radius, $r_{\text{mean}} = 0.65$; standard deviation, $\sigma = 0.1$.

law were $n_p = 1.07$ and $n_p' = 0.0002$, Junge exponent ξ was 3.2, the refractive indices of the lognormal mode of the particles were $m_p = 1.17$ and $m_p' = 0.007$ at 443 nm and $m_p' = 0.0005$ at 490 nm, the mean radius was $r_{\text{mean}} = 0.65$ μm, and the standard deviation was $\sigma = 0.1$ μm. The relative RMS obtained for $R_{443/555}$ and $R_{490/555}$ was 9.1% and 7.6%, respectively (Table 3). Except in the near-forward region ($\theta < 5°$), the agreement is satisfactory, especially at 20° and 160°, where the minima are properly reproduced. Furthermore, the order of magnitude of the refractive indices derived for both types of particle ($n_p < 1.10$ in the case of a Junge distribution and $m_p > 1.12$ in the case of the modal distribution) suggests that a phytoplankton population coexisted with an absorbing mineral suspension. The occurrence of a continuous background of phytoplankton (i.e., distributed according to a Junge power law) is realistic because a high Chl *a* was measured in the second half of the experiment, in particular on 11 August at 16 m (Chl $a = 1.85$ mg m^{-3}). The weak value of Junge exponent ξ points out the occurrence of large cells, which is consistent with the higher packaging effect observed after 6 August.[32] The presence of minerals is corroborated by the values of $\tilde{b}_{bp}(\tilde{b}_{bp} \sim 2\%)$, which were too high to be ascribed to phytoplankton.[32] The relatively high value of m_p' at 443 nm is in agreement with significant absorption by nonalgal particles [$a_{\text{NAP}}(443\text{ nm}) = 0.07$ m^{-1}]. The fact that the minerals consist of submicrometric particles ($r_{\text{mean}} = 0.65$ μm) can be explained by effect of the bottom, which is composed mainly of sand. We note that bubbles also lead to high values of $\tilde{b}_{bp}$.[11] However, their signature is not present in the VSF measurements. The most significant feature of the angular scattering distribution by bubbles appears in the range of scattering of angles 60°–80°, where the magnitude of the scattering is higher by 1 order of magnitude than the scattering by other particles.[11] Therefore the effects of bubbles (clean or coated bubbles) can easily be observed in this angular domain. Introduction of bubbles into the Mie calculations has always led to large discrepancies in the retrieval of $R_{443/555}$ in the 60°–80° range. We conclude that bubbles do not contribute significantly to the angular variation of $R_{443/555}$ in this experiment.

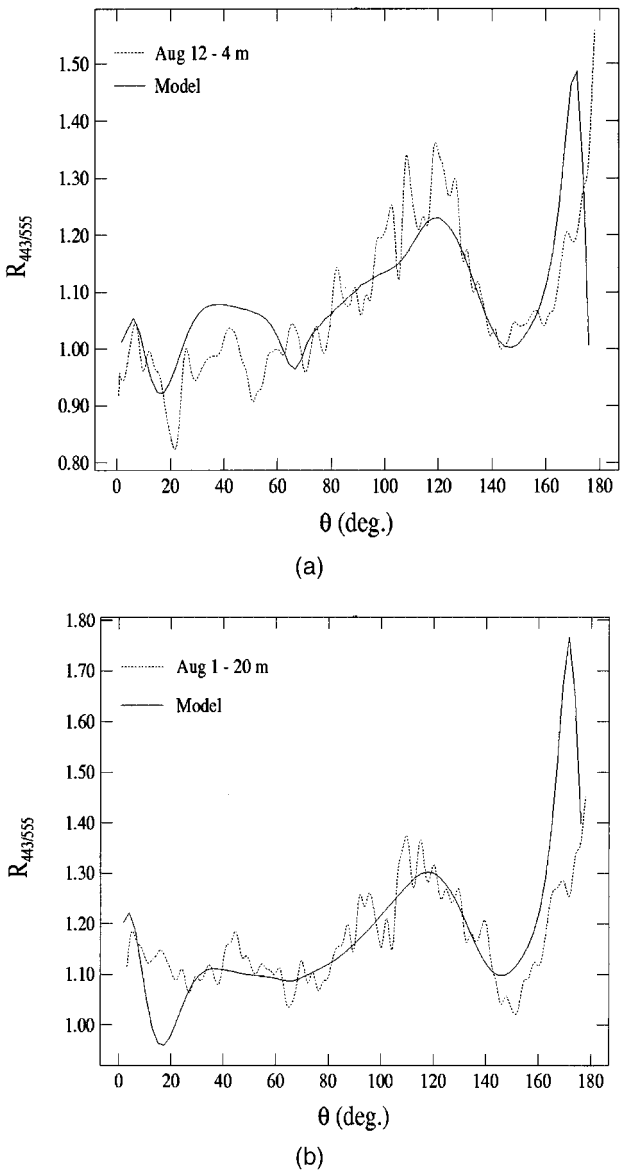

Fig. 12. Retrieval of $R_{443/555}$ with Mie theory on (a) 12 August at 4 m, (b) 1 August at 20 m. The parameters used to retrieve the observations are listed in Table 2.

The retrieval of the spectral ratios $R_{443/555}$ and $R_{490/555}$ was also successful for the data measured on 12 August at 4 m and 1 August at 20 m (Table 1 and Fig. 12). For clarity, Fig. 12 shows only the retrieval

Table 2. Parameters of Mie Computations Used to Retrieve Spectral Ratio $R_{443/555}$ on 1 August at 20 m and 12 August at 4 m[a]

Date (Depth [m])	Junge Distribution (n_p–in_p')	Junge Exponent ξ	Lognormal Distribution (n_p–im_p')[a]
1 August (20)	1.05–i0.0005	3.6	1.17–i0.000
12 August (4)	1.05–i0.0015	3.2	1.17–i0.0005

[a]The value of r_{mean} in both cases is 0.6; that of σ is 0.15.

of $R_{443/555}$. For both samples, the main angular features found in the measurements were well retrieved, especially the minima observed at 20° and 160° (especially on 12 August) and the maximum near 120°. The Mie parameters that allowed us to obtain the best agreement are listed in Table 2. As for measurements on 11 August, the Mie parameters suggest the coexistence of phytoplanktonic and mineral particles on 1 and 12 August. This result is consistent with the observations, as Chl a was significant both days (Chl a = 1.8 mg m^{-3} on 12 August and Chl a = 1.2 mg m^{-3} on August 1). The backscattering ratio was also sufficiently high (>2%) to justify the occurrence of minerals. Note that a_{NAP}(443 nm) was least on 1 August at 20 m (<0.02 m^{-1}), which is consistent with the retrieval of nearly nonabsorbing particles.

The presence of monodispersed particles was expected from the spectral variation observed in $\tilde{b}_{bp}$ during the experiment. The spectral ratio $\tilde{b}_{bp}$ of 443 to 555 nm varied within ±30%.[32] According to previous studies based on measurements of algae cultures,[43,53] such a significant spectral variation can be ascribed to the presence of monodispersed particles.

Our study showed that the variations of the measured β_p spectra with respect to the scattering angle were well reproduced from theory by use of realistic parameters. Such a validation was necessary owing to the lack of identical spectral measurements of the VSF in the literature. Based on our analysis, the spectral shapes of β_p and their variations with scattering angle are highly sensitive both to absorption effects and to the size distribution of the particles.

C. Spectral Variation of the Particulate Phase Function

Previous studies[15,17] showed that particulate phase function $\tilde{\beta}_p(\theta)$ is weakly wavelength dependent. However, it is worth noting that the conclusions were drawn on the basis of a limited number of samples, typically fewer than 20, and with equipment dating from three decades ago. Owing to the lack of recent spectral measurements of $\tilde{\beta}_p(\theta)$, a spectrally neutral variation of $\tilde{\beta}_p(\theta)$ is still currently assumed in the radiative-transfer computations[38,54] and in the ocean color inversion algorithms.[55] Such a hypothesis might be justified because β_p and b_p are both highly dependent on the wavelength; thus, one can expect that their ratio will significantly reduce the spectral effects. Our experiment allowed us to test the reliability of the independence of $\tilde{\beta}_p$ from wavelength, at least in the Crimea Peninsula. First we studied the

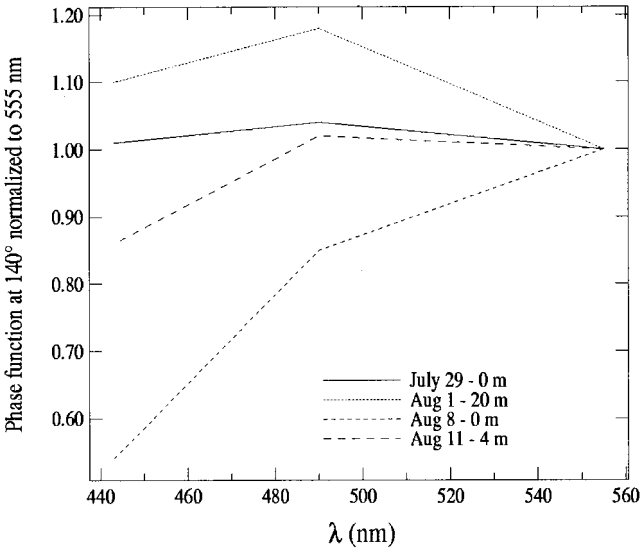

Fig. 13. Spectral variation of the phase function of the particles at 140° normalized to 555 nm measured on four days.

spectral variation of $\tilde{\beta}_p$ at 140° (Fig. 13). As was observed for β_p (Fig. 2), $\tilde{\beta}_p$ spectra showed a high degree of spectral variability during the experiment. A depression was observed in the blue relative to the green on certain days (for example, on 8 August at 0 m). As β_p(140°) spectra were observed to be sensitive to the absorption effects, we examined the relationship between $\tilde{\beta}_p$(140°) and the absorption coefficients of the particles. Two significant correlations (r^2 = 0.71 in both cases) were found between the phase function at 443 nm and a_{NAP}(400 nm) before and after 6 August (Fig. 14). Therefore the phase function at 140° is also sensitive to the absorption effects. The

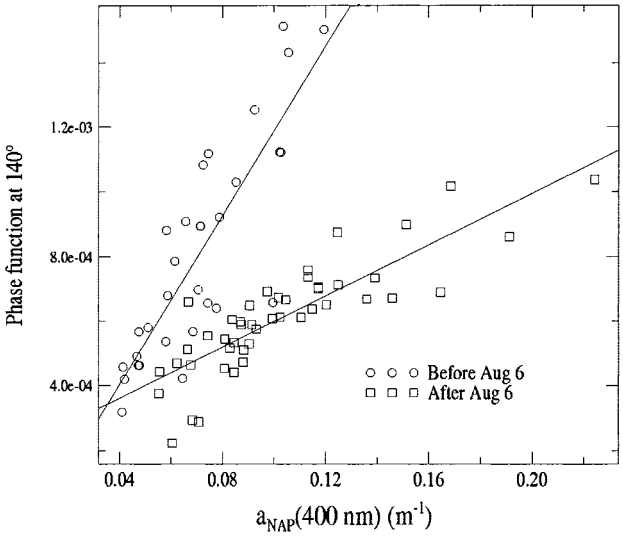

Fig. 14. Relationship of $\tilde{\beta}_p$(140) at 443 nm to the absorption coefficient of nonalgal particles a_{NAP} at 400 nm. Equations for linear fit: before 6 August, $\tilde{\beta}_p$(140°, 443 nm) = 0.0110 a_{NAP}(400 nm); r^2 = 0.71. After 6 August, $\tilde{\beta}_p$(140°, 443 nm) = 0.0038 a_{NAP}(400 nm) + 0.0002; r^2 = 0.71.

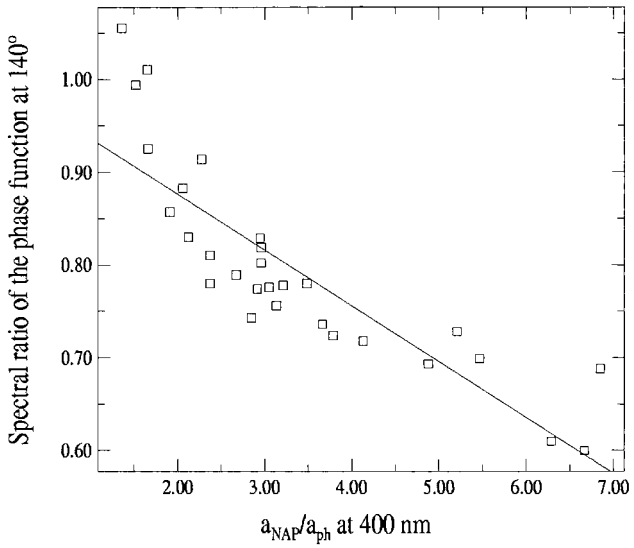

Fig. 15. Spectral ratio $\beta_p(140°)$ from 443 to 555 nm, i.e., $R_{443/555}(140°)$, in surface layer 0–4 m as a function of parameter a_{NAP}/a_{ph} at 400 nm. Equation for the linear fit, $R_{443/555}(140°) = -0.060\ a_{NAP}/a_{ph}(400\text{ nm}) + 0.99$; $r^2 = 0.72$.

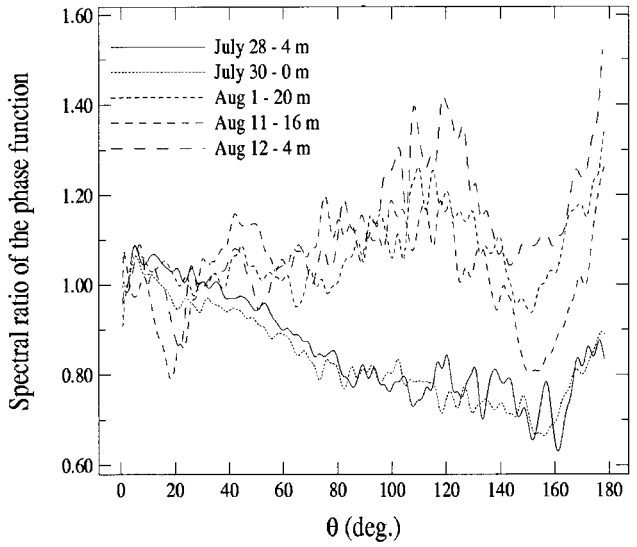

Fig. 16. Dependence of spectral ratio of the phase function from 443 to 555 nm, $\tilde{R}_{443}$, on scattering angle as measured on 28 July at 4 m, 30 July at 0 m, 1 August at 20 m, 11 August at 16 m, and 12 August at 4 m.

slopes of the two linear fits differed by a factor of 3, thus supporting the change in particle type after the gusting wind observed during the experiment.

The following study of the spectral variation of $\tilde{\beta}_p(140°)$ focuses only on the layer 0–4 m, which was most influenced by the weather changes. The spectral ratio of $\tilde{\beta}_p$ from 443 to 555 nm (hereafter referred to as $\tilde{R}_{443}$) at 140° was related to the parameter a_{NAP}/a_{ph} measured at 400 nm (Fig. 15). Figure 15 allows us to evaluate the relative contribution of nonalgal particles and phytoplankton absorption to the spectral variation of $\tilde{\beta}_p(140°)$. A significant correlation was observed ($r^2 = 0.72$): $\tilde{R}_{443}(140°)$ decreased linearly from 1.05 to 0.60 with a_{NAP}/a_{ph}. Therefore the phase function at 140° showed a greater depression in the blue when the absorption by nonalgal particles was greater than phytoplankton absorption (i.e., high values a_{NAP}/a_{ph}). The lowest values of $\tilde{R}_{443}(140°)$ (i.e., the highest spectral variation) were observed on 6 and 8 August, when the contribution of a_{NAP} to total particulate absorption a_p was 66% and 88%, respectively. $\tilde{\beta}_p(140°)$ spectra flattened [$\tilde{R}_{443}(140°) \rightarrow 1$], however, when the relative importance of phytoplankton absorption increased. Large particles typically induce a weak spectral variation of the backscattering properties.[56] Because phytoplankton cells are usually larger than nonalgal particles, it is not surprising to observe a flattening of the $\tilde{\beta}_p(140°)$ spectra as a_{NAP}/a_{ph} decreases.

According to the definition of the phase function [Eq. (3)], the spectral ratio of $\tilde{R}_{443}$, expressed in terms of spectral ratio $R_{443/555}$, is written as

$$\tilde{R}_{443} = R_{443}\,\frac{b_p(555\text{ nm})}{b_p(443\text{ nm})}. \tag{11}$$

The ratio $b_p(555\text{ nm})/b_p(443\text{ nm})$ is independent of the scattering angle; thus the angular shapes expected are the same as for the VSF, to a scaling factor given by $b_p(555\text{ nm})/b_p(443\text{ nm})$ (Fig. 16). Thus the conclusion about the sensitivity of the angular variations of the spectral shapes to the absorption and the size distribution of particles is the same for $\tilde{R}_{443}$. However, in the presence of highly absorbing particles, the depression of the phase function in the blue is more pronounced [$b_p(555\text{ nm})/b_p(443\text{ nm}) > 1$] than the depression observed in the VSF.

4. Conclusions

Spectral measurements of the volume scattering function were collected in a coastal environment. For the first time to our knowledge, the spectral variations of both the volume scattering function and the phase function of the particles were analyzed as a function of scattering angle. We examined the VSF at 140° because it is often used to derive the backscattering coefficient of the particles. The data showed lower values of $\tilde{\beta}_p(140°)$ at 443 nm relative to 555 nm, especially in the second half of the field experiment, which were ascribed to the occurrence of absorbing nonalgal particles in the study area. The angular distribution of the spectral ratio of the VSF showed intricate features. Three trends prevailed during the experiment: (i) a monotonic decrease with θ, (ii) minima near 20° and 160°, and (iii) a maximum near 120°. Besides using absorption effects, the only way to reconcile the observations with theory was to assume that the size distribution of the particles was the sum of a Junge power law and a lognormal function. In particular, the introduction of a modal distribution of the particles allowed us to retrieve successfully the minima and maxima observed in the spectral ratio of the VSF. Despite the

fact that we were unable to validate rigorously the absolute values of the parameters derived from theory, the order of magnitude of the retrieved complex refractive index was consistent with other ancillary optical data, such as the chlorophyll *a* concentration and the magnitude of the backscattering ratio. The occurrence of monodispersed particles was also consistent with the high spectral variability observed in the backscattering ratio.

In a fashion similar to that for β_p, the spectral variation of the particulate phase function was highly dependent on the scattering angle. The angular variation of $\tilde{\beta}_p$ spectra was similarly sensitive to the absorption effects and to the size distribution of particles. Therefore our results suggest caution in the use of spectrally neutral phase functions in radiative-transfer modeling. We measured departure as far as 40% from flatness at 140°. As a result of this study, future efforts should be directed toward routine spectral measurements of the VSF over the full range of scattering angles for better understanding of the directional effects of the particles and thus for proper prediction of the water leaving signal for remote sensing purposes.

Appendix A. Notation and Abbreviations Used in This Paper

a_{NAP}	Nonalgal particles absorption coefficient (m^{-1})
a_{ph}	Chlorophyll *a* absorption coefficient (m^{-1})
a_p	Total particulate absorption coefficient (m^{-1})
b_p	Particulate scattering coefficient (m^{-1})
b_{bp}	Particulate backscattering coefficient (m^{-1})
$\tilde{b}_{bp}$	Particulate backscattering ratio (i.e., b_{bp}/b_p)
$\beta_p(\lambda, \theta)$	Particulate volume scattering function ($m^{-1}sr^{-1}$)
c	Attenuation coefficient (m^{-1})
c_p	Particulate attenuation coefficient (m^{-1})
Chl *a*	Chlorophyll *a* concentration (mg m^{-3})
λ	Wavelength (nm)
n_p	Real part of the refractive index of the particles distributed according to the Junge power law
n_p'	Imaginary part of the refractive index of the particles distributed according to the Junge power law
m_p	Real part of the refractive index of the particles lognormally distributed
m_p'	Imaginary part of the refractive index of the particles lognormally distributed
$\tilde{\beta}(\theta)$	Phase function
$\tilde{\beta}_p(\theta)$	Phase function of the particles
θ	Scattering angle (degree)
Q_{bb}	Backscattering efficiency factor (ratio of radiative energy backscattered by the particle to the energy impinging on the geometrical cross section of the same particle)
r_{mean}	Mean radius of the lognormal size distribution
σ	Standard deviation
$R_{443/555}(\theta)$	Spectral ratio $\beta_p(\theta, 433\ \mathrm{nm})/\beta_p(\theta, 555\ \mathrm{nm})$
$R_{490/555}(\theta)$	Spectral ratio $\beta_p(\theta, 490\ \mathrm{nm})/\beta_p(\theta, 555\ \mathrm{nm})$
$\tilde{R}_{443}$	Spectral ratio $\tilde{\beta}_p(\theta, 443\ \mathrm{nm})/\tilde{\beta}_p(\theta, 555\ \mathrm{nm})$
VSF	Volume scattering function
ω_p	Single scattering albedo of the particles (i.e., b_p/c_p)
ξ	Junge exponent of the size distribution of the particles

This study was supported by the Centre National d'Etudes Spatiales (France) in the framework of the Colour Observations for Validation of remote Sensing algorithms (COBRA) project (contract N02/CNES/4800000051). The authors are grateful to Gallina Berseneva and Tatiana Churilova for processing the absorption data. We thank Alexander Kuznetsov, Nicolay Spichak, and Apollon Kuklin for providing technical help with the platform for data acquisition. We are also grateful to Y. Huot for helpful discussions and valuable remarks on the manuscript. We thank the reviewers for their useful comments and suggestions.

References

1. M. S. Twardowski, E. Boss, J. B. Macdonald, W. S. Pegau, A. H. Barnard, and J. R. V. Zaneveld, "A model for estimating bulk refractive index from the optical backscattering ratio and the implications for understanding particle composition in case I and case II waters," J. Geophys. Res. **106,** C7, 14,129–14,142 (2001).
2. O. B. Brown and H. R. Gordon, "Comment on method for the determination of the refractive index of particles suspended in the ocean," J. Opt. Soc. Am. **63,** 1616–1617 (1973).
3. O. B. Brown and H. R. Gordon, "Size-refractive index distribution of clear coastal water particulates from light scattering," Appl. Opt. **13,** 2874–2881 (1974).
4. J. R. V. Zaneveld and H. Pak, "The determination of the index of refraction of particles suspended in the ocean," J. Opt. Soc. Am. **63,** 321–324 (1973).
5. J. R. V. Zaneveld, D. M. Roach, and H. Pak, "The determination of the index of refraction distribution of oceanic particulates," J. Geophys. Res. **79,** 4091–4095 (1974).
6. D. M. Roach, "Determination of refractive index distributions for oceanic particulates," Ph.D. dissertation (Oregon State University, 1974).
7. R. W. Spinrad and J. F. Brown, "Relative real refractive index of marine microorganisms: a technique for flow cytometric estimation," Appl. Opt. **25,** 1930–1934 (1986).
8. S. G. Ackleson and R. W. Spinrad, "Size and refractive index of individual marine particulates: a flow cytometric approach," Appl. Opt. **27,** 1270–1277 (1983).
9. A. Bricaud, C. Roesler, and J. R. V. Zaneveld, "*In situ* methods for measuring the inherent optical properties of ocean waters," Limnol. Oceanogr. **40,** 393–410 (1995).
10. E. Boss, W. S. Pegau, M. Lee, M. Twardowski, E. Shybanov, G. Korotaev, and F. Baratange, "Particulate backscattering ratio at LEO 15 and its use to study particle composition and

distribution," J. Geophys. Res. **109,** C01014, doi:10.1029/2002JC001514 (2004).
11. X. Zhang, M. Lewis, M. E.-G. Lee, B. Johnson, and G. K. Korotaev, "The volume scattering function of natural bubble populations," Limnol. Oceanogr. **47,** 1273–1282 (2002).
12. X. Zhang, M. Lewis, W. P. Bissett, B. Johnson, and D. Kohler, "Optical influence of ship wakes," Appl. Opt. **43,** 3122–3132 (2004).
13. O. S. Ulloa, S. Sathyendranath, and T. Platt, "Effect of the particle-size distribution on the backscattering ratio in seawater," Appl. Opt. **33,** 7070–7077 (1994).
14. J. E. Tyler and W. H. Richardson, "Nephelometer for the measurement of volume scattering *in situ,*" J. Opt. Soc. Am. **48,** 354–357 (1958).
15. T. J. Petzold, "Volume scattering functions for selected ocean waters," Tech. Rep. 72-28 (Scripps Institute of Oceanography, 1972).
16. G. Kullenberg, "Observed and computed scattering functions," in *Optical Aspects of Oceanography,* N. G. Jerlov and E. S. Nielsen, eds (Academic, 1974), pp. 25–49.
17. A. Morel, "Diffusion de la lumière par les eaux de mer: résulats expérimentaux et approche théorique," in *Optics of the Sea,* NATO AGARD, Lecture Series 61 (NATO Advisory Group for Aerospace Research and Development, 1973), pp. 3-1-1–3-1-76.
18. C. D. Mobley, B. Gentili, H. R. Gordon, Z. Jin, G. W. Kattawar, A. Morel, P. Reinsersman, K. Stamnes, and R. H. Stavn, "Comparison of numerical models for computing underwater light fields," Appl. Opt. **32,** 7484–7505 (1993).
19. K. L. Carder, R. D. Tomlinson, and G. F. Beardsley, Jr., "A technique for the estimation of indices of refraction of marine phytoplankters," Limnol. Oceanogr. **17,** 833–839 (1972).
20. E. Aas, "Refractive index of phytoplankton derived from its metabolite composition," J. Plankton Res. **18,** 2223–2249 (1996).
21. D. Stramski, A. Morel, and A. Bricaud, "Modeling the light attenuation and scattering by spherical phytoplankton cells: a retrieval of the bulk refractive index," Appl. Opt. **27,** 3954–3956 (1988).
22. K. L. Carder, P. R. Betzer, and D. W. Eggimann, "Physical, chemical and optical measures of suspended particle concentrations: their intercomparison and application to the West African shelf," in *Suspended Solids in Water,* R. J. Gibbs, ed. (Plenum, 1974), pp. 173–193.
23. D. R. Lide, "Physical and optical properties of minerals," in *CRC Handbook of Chemistry and Physics,* 77th ed. D. R. Lide, ed. (CRC, 1997), pp. 4.130–4.136.
24. H. Bader, "The hyperbolic distribution of particles sizes," J. Geophys. Res. **75,** 2822–2830 (1970).
25. R. W. Sheldon A. Prakash, and W. H. Sutcliffe, Jr., "The size distribution of particles in the ocean," Limnol. Oceanogr. **17,** 327–340 (1972).
26. J. C. Kitchen, "Particle size distribution and the vertical distribution of suspended matter in the upwelling region off Oregon," Rep. 77-10 (Oregon State University, 1977).
27. O. V. Kopelevich, "Small parameter model of optical properties of sea water," in *Physical Ocean Optics,* Vol. 1 of Ocean Optics, A. S. Monin, ed. (Nauka, Moscow, 1983; in Russian), Chap. 8, pp. 208–234.
28. V. I. Haltrin and G. Kattawar, "Light fields with Raman scattering and fluorescence in sea water," Tech. Rep. (Texas A&M U. Press 1991).
29. D. Risovic, "Two-component model of sea particle size distribution," Deep-Sea Res. Part I **40,** 1459–1473 (1993).
30. R. A. Maffione and D. R. Dana, "Instruments and methods for measuring the backward-scattering coefficient of ocean waters," Appl. Opt. **36,** 6057–6067 (1997).
31. M. E. Lee and M. R. Lewis, "A new method for the measurement of the optical volume scattering function in the upper ocean," J. Atmos. Ocean. Technol. **20,** 563–571 (2003).
32. M. Chami, E. B. Shybanov, T. Y. Churilova, G. A. Khomenko, M. E.-G. Lee, O. V. Martynov, G. A. Berseneva, and G. K. Korotaev, "Optical properties of the particles in the Crimea coastal waters (Black Sea)," J. Geophys. Res. (to be published).
33. G. S. Fargion and J. L. Mueller, "Ocean optics protocols for satellite ocean color sensor validation, revision 2," NASA Tech. Memo. 2000–209966 (NASA Goddard Space Flight Center, 2000).
34. O. Holm-Hansen, C. J. Lorenzen, R. W. Holmes, and J. D. H. Strickland, "Fluorometric determination of chlorophyll," J. Cons. Intl. Explor. Mer. **30,** 3–15 (1965).
35. C. S. Yentsch, "Measurement of visible light absorption by particulate matter in the ocean," Limnol. Oceanogr. **7,** 207–217 (1962).
36. B. G. Mitchell and D. A. Kiefer, "Chlorophyll *a* specific absorption and fluorescence excitation spectra for light limited phytoplankton," Deep Sea Res. **35,** 639–663 (1988).
37. M. Kishino, N. Takahashi, N. Okami, and S. Ichimura, "Estimation of the spectral absorption coefficients of phytoplankton in the sea," Bull. Marine Sci. **37,** 634–642 (1985).
38. C. D. Mobley, L. K. Sundman, and E. Boss, "Phase function effects on oceanic light fields," Appl. Opt. **41,** 1035–1050 (2002).
39. A. Morel, "Optical properties of pure water and pure seawater," in *Optical Aspects of Oceanography,* N. G. Jerlov and E. S. Nielsen, eds. (Academic, (1974), pp. 1–24.
40. E. Boss and W. S. Pegau, "Relationship of light scattering at an angle in the backward direction to the backscattering coefficient," Appl. Opt. **40,** 5503–5507 (2001).
41. T. Oishi, "Significant relationship between the backward scattering coefficient of seawater and the scattering at 120°," Appl. Opt. **29,** 4658–4665 (1990).
42. A. Bricaud and A. Morel, "Light attenuation and scattering by phytoplanktonic cells. A theoretical modeling," Appl. Opt. **25,** 571–580 (1986).
43. Y. H. Ahn, A. Bricaud, and A. Morel, "Light backscattering efficiency and related properties of some phytoplankters," Deep Sea Res. Part I, **39,** 1835–1855 (1992).
44. M. Babin, A. Morel, V. Fournier-Sicre, F. Fell, and D. Stramski, "Light scattering properties of marine particles in coastal and open ocean waters as related to the particle mass concentration," Limnol. Oceanogr. **48,** 843–859 (2003).
45. H. C. van de Hulst, *Light Scattering by Small Particles* (Wiley, 1957).
46. R. P. Bukata, J. H. Jerome, K. Y. Kondratyev, and D. V. Pozdnyakov, *Optical Properties and Remote Sensing of Inland and Coastal Waters* (CRC Press, 1995).
47. S. Tassan and G. M. Ferrari, "An alternative approach to absorption measurements of aquatic particles retained on filters," Limnol. Oceanogr. **40,** 1358–1368 (1995).
48. D. G. Bowers, G. E. L Harker, and B. Stephan, "Absorption spectra of inorganic particles in the Irish Sea and their relevance to remote sensing of chlorophyll," Int. J. Remote Sens. **17,** 2449–2469 (1996).
49. M. Babin and D. Stramski, "Light absorption by aquatic particles in the near infra-red spectral region," Limnol. Oceanogr. **47,** 911–915 (2002).
50. K. L. Carder, G. F. Beardsley, and H. Pak, "Particle size distribution in the Eastern Equatorial Pacific," J. Geophys. Res. **76,** 5070–5077 (1971).
51. H. R. Gordon and O. B. Brown, "A theoretical model of light scattering by Sargasso Sea particles," Limn. Oceanogr. **17,** 826–832 (1972).
52. M. Jonasz, "Particle size distribution in the Baltic," Tellus **35B,** 346–358 (1983).
53. A. Morel and A. Bricaud, "Theoretical results concerning light ab-

sorption in a discrete medium, and application to specific absorption of phytoplankton," Deep Sea Res, Part I **28,** 1375–1393 (1981).
54. A. Morel and B. Gentili, "Diffuse reflectance of oceanic waters: its dependence on Sun angle as influenced by the molecular scattering contribution," Appl. Opt. **30,** 4427–4438 (1991).
55. C. S. Roesler and E. Boss, "Spectral beam attenuation coefficient retrieved from ocean color inversion," Geophys. Res. Lett. **30,** 1468, doi:10.1029/2002GL016185 (2003).
56. A. Morel and S. Maritorena, "Bio-optical properties of oceanic waters: a reappraisal," J. Geophys. Res. **106,** C4, 7163–7180 (2001).